Applied Clay Science 216 (2022) 106311

Contents lists available at ScienceDirect

Applied Clay Science

journal homepage: www.elsevier.com/locate/clay

Research Paper

Review and new data on the surface properties of palygorskite: A comparative study

Mercedes Suárez [a,*], Javier García-Rivas [a], Juan Morales [a], Adrián Lorenzo [a], Andrea García-Vicente [a], Emilia García-Romero [b,c]

[a] Department of Geology, University of Salamanca, Plaza de la Merced s/n, Salamanca 37008, Spain
[b] Department of Mineralogy and Petrology, Complutense University of Madrid, C/José Antonio Novais 12, Madrid 28040, Spain
[c] Geosciences Institute, Spanish Research Council and Complutense University of Madrid, C/José Antonio Novais 12, Madrid 28040, Spain

ARTICLE INFO

Keywords:
Palygorskite
Specific surface area
Microporosity
External area
Microstructure

ABSTRACT

Palygorskite is a mineral used in a wide number of industrial sectors. Currently, there are hundreds of studies in which palygorskite is a part of different nanocomposites and bionanocomposites. The surface properties are essential for these applications, and in this work, an in-depth revision of these properties is done, showing that the high variability found cannot be explained only by the number of impurities or by differences in the analysis conditions. To further deepen the knowledge of the surface properties of palygorskite and palygorskitic clays, a comparative study of a wide group of high purity samples is also performed, and new data on these surface properties are provided with the determination of the specific surface area (SSA), micropore surface area ($SSA_{\mu p}$), micropore volume ($V_{\mu p}$), external surface area (SSA_{Ex}), and mean equivalent pore diameter. Both the bibliographic data and new data show that SSA varies from a few tens of m^2g^{-1} to almost 300 m^2g^{-1}, and the microporosity and external surface proportions also vary greatly. The experimental data obtained show that 1) ordinary soft vacuum conditions produce structural folding, which limits the accessibility to the inner part of the structural tunnels; 2) microporosity is related to the intra- and inter-fibre microporosity, depending first on the fibre size, because the shorter the fibre, the higher the partial accessibility to the entrance of the channels; 3) the crystal chemistry of the samples also influences the SSA because the Mg-rich terms, which have higher content of sepiolite polysome proportions in their structure as well as wider and more accessible intracrystalline channels than palygorskite polysomes.

1. Introduction

Palygorskitic clays are rocks rich in palygorskite, and they have industrial interest owing to the physical-chemical properties of this fibrous clay. Palygorskite is the aluminic term of the sepiolite-palygorskite polysomatic series (Suárez and García-Romero, 2011, 2013), in which tunnels are located inside of the crystals and channels on the surface, all running parallel to the fibre, which result in a high surface area. In recent decades, the uses of and research on the application properties of palygorskite have changed from raw materials to highly specialized products. From its use as a granular absorbent, only after grinding or soft acid treatment and as products of the first or second generations (Suárez-Barrios et al., 1995; Vicente-Rodríguez et al., 1996; Chen et al., 2007), to the design of nanocomposites or bionanocomposites (Ruiz-Hitzky et al., 2013a, 2013b; Wang and Wang, 2016; Tavanaee et al., 2017) as products of the fifth or sixth generations (Álvarez et al., 2011), research on this mineral has grown exponentially in recent years. These clays are used not only in pharmaceutics and cosmetic products (López-Galindo et al., 2007, 2011) but also for the removal of pharmaceuticals from wastewater (Chang et al., 2019). Palygorskitic clays have also been studied for other environmental applications, such as adsorbents of dyes (Mu and Wang, 2016; Zhang et al., 2020) and heavy metals (Oubagaranadin and Murthy, 2011; Bourliva et al., 2018; Tichapondwa and Van Biljon, 2019). Related to animal and human health, this clay mineral has been studied for the preparation of green antibacterials to replace synthetic antibiotics (Liu et al., 2020; Zhong et al., 2020). On the other hand, Juárez et al. (2016) and López-Pacheco et al. (2017) suggested the potential use of palygorskite as a therapeutic tool against inflammatory diseases.

All these applications are based on the physical-chemical properties

* Corresponding author.
E-mail address: msuarez@usal.es (M. Suárez).

https://doi.org/10.1016/j.clay.2021.106311
Received 1 July 2021; Received in revised form 11 October 2021; Accepted 17 October 2021
Available online 28 November 2021

of palygorskite, mainly on its specific surface area and its ability as a granular absorbent and adsorbent. The data of the specific surface area of palygorskite are obtained from the application of the BET method (Brunauer et al., 1938) to the isotherms of N_2 adsorption, and it is difficult to establish comparisons among samples from different sources because of 1) the difference among the experimental conditions used in the analysis and 2) the amount and type of impurities contained by the samples studied in the different works.

The specific surface area and the ab/adsorption capacity of the clay minerals are related to the crystal structure and crystal defects, the small size of crystals and their laminar or fibrous morphology. Furthermore, the microstructures of clay minerals are related, according to comparative studies on wide groups of samples analysed under the same conditions conducted by Rutherford et al. (1997), Kaufhold et al. (2010) on bentonites and Suárez and García-Romero (2012) and Suárez et al. (2016) on sepiolite. To our knowledge, no comparative study has been performed on palygorskite, and the aim of this work is to complete an in-depth examination of the literature and study the surface properties of a group of very pure palygorskites to determine the variability of these properties and what they depend on.

1.1. *The specific surface area and other textural properties of palygorskite and palygorskitic clays*

Table 1 contains the results of textural parameters, including the specific surface area, of palygorskites and palygorskitic clays deduced from the N_2 isotherms and obtained from bibliographical research. Only high purity sample data were chosen for this comparative analysis. As in most cases, the amount of palygorskite in palygorskitic clays is not reported, so the sample purity has been estimated from the X-ray diffraction (XRD) patterns that appear in the corresponding article. Therefore, the term "high purity of palygorskite" is used in this study when the intensities of the main mineral reflections that appear as impurities are low and other reflections are not visible among the palygorskite reflections or they have very low intensity. The most frequent impurities are quartz and carbonates, mainly dolomite; although, calcite also appears on some occasions. Although not observed very frequently, other clay minerals, such as smectites, illite and kaolinite, also appear in small amounts, and in that case, they can contribute to the specific surface area, especially if smectites. In Table 1, the data show samples with only minor amounts of other clay minerals.

Several textural parameters can be obtained from the analysis of the N_2 isotherm. The first is the specific surface area, which can be calculated using different methods, such as the BET equation model and the Langmuir equation, with BET being the most commonly used. In addition to the specific surface area, other textural parameters, such as the micropore surface area, external surface area, micropore volume, total pore volume and mean pore diameter can be calculated from the isotherms of N_2. On very few occasions, all the aforementioned parameters are reported (Table 1).

The specific surface area reported for palygorskite ranges between 60 m^2g^{-1} and 279 m^2g^{-1}, according to Frini-Srasra and Srasra (2010) and Papoulis et al. (2013), respectively. Exceptionally, lower values have been reported for palygorskitic clays with high contents of impurities. The frequency of the BET values is plotted (Fig. 1 a) and follows a normal distribution around the mean value of 152 m^2g^{-1}, with a wide standard deviation of ~50 m^2g^{-1}. These results show a wide variability in the specific surface area of this fibrous mineral, although a direct comparison among these results cannot be done because of the differences in 1) the pre-treatments applied to the samples, including the outgassing conditions used, and 2) the presence of different amounts of and type of impurities, as summarized in Table 1. It is literally impossible to analyse the influence of the pre-treatments and the impurities because in many cases, this information is not given and when it is known, there are very large differences among the data.

Regarding the pre-treatments, the following two groups of data were obtained: those from powdered samples of different sizes, frequently unknown, and those from the <2 μm and < 45 μm fractions obtained from the suspensions in water, dried and powdered. The specific surface area of the samples for which there is information on the pre-treatment is plotted by grouping the samples according to the fraction or particle size (Fig. 2). As can be observed, the variability remains inside each group, and the particle size does not seem to be relevant. In fact, in the group of samples obtained from suspensions of the clay in water and separation of the <2 μm fraction, in which the original microstructure has been modified, there are samples with values between 75 m^2g^{-1} (Ghrab et al., 2018) and 279 m^2g^{-1} (Papoulis et al., 2013), the highest referred for palygorskite.

In addition to the sample preparation, which obviously plays an important role because it can change the microstructure of the sample, the outgassing conditions must be considered in the comparative data analysis. The outgassing process is necessary to desorb the species that are naturally physisorbed and to clean the mineral surface prior to N_2 adsorption. For that, the sample must be heated in vacuum until a low residual pressure is reached, especially for microporous materials such as palygorskite. According to the International Union of Pure and Applied Chemistry (IUPAC) recommendations (Thommes et al., 2015), pressures <1 Pa are desirable to be able to measure the microporosity. Although the outgassing conditions are very important, only a quarter of the works collected in Table 1 give information on the outgassing process before the N_2 adsorption, and these conditions are widely variable. No two studies used the same conditions. The following three temperature ranges used by the different authors that can be considered according to the thermal behaviour of palygorskite: under 120 °C, between 120 °C and 250 °C, and between 300 °C and 400 °C; furthermore, there is no correlation between the outgassing temperature and the SSA values (Fig. 3). These temperatures correspond to the loss of absorbed, zeolitic and the first half of coordinated water, respectively, at atmospheric pressure (Serna et al., 1977; VanScoyoc et al., 1979; Suárez and García-Romero, 2019). If a vacuum was not considered, a temperature of approximately 200 °C would be the ideal temperature for 1) evacuating all the absorbed and zeolitic water without affecting the coordinated water, which implies structural folding, and 2) guaranteeing full accessibility to N_2 to the interior of the channels. However, outgassing is performed under a vacuum, and the sum of the vacuum to the heating decreases the temperature required to evacuate the different water types. According to the data recorded in Table 1 and considering that there are no SSA value variations among the three temperatures ranges, as pointed out before, it could be assumed that the effect of vacuum is higher than that of temperature; furthermore, all samples achieved similar structural conditions, which probably implied the structural folding. This observation agrees with observations by Cases et al. (1991), who found that the SSA of palygorskite decreases under a vacuum and thermal treatment over 70 °C due to a partial loss of microporosity related to the structural folding.

It is well known that the SSA of sepiolite and palygorskite originates from the sum of the microporosity and the external surface. Although most authors relate the microporosity of palygorskite to its structural zeolitic channels, Cases et al. (1991) showed that a part of the microporosity is due to inter-fibre porosity and depends on the microstructure. The microstructure, and consequently the microporosity and SSA of a sample, can change with sample pre-treatment, such as suspension in water or soft acid treatment, as demonstrated for sepiolite by Suárez and García-Romero (2012). In any case, the microstructure is a characteristic of each sample that depends on its geological genetic process (García-Romero and Suárez, 2013) and laboratory procedures. However, these are not considered in most studies in which the SSA and microporosity of palygorskite are measured in natural powdered samples to be compared afterwards to treated samples by procedures that imply modification of the microstructure. The modifications found are always interpreted without considering the effect of the microstructure modification.

Only 33% of the studies recorded in Table 1 provide microporosity

Table 1
Resume of the bibliographic review. Note the wide dispersion of both of the values of the different textural parameters as the data provide in each reference.

Geographical origin	SSA_{BET} ($m^2\ g^{-1}$)	$SA_{\mu p}$ ($m^2\ g^{-1}$)	SA_{ext} ($cm^2\ g^{-1}$)	$V_{\mu p}$ ($cm^3\ g^{-1}$)	Vt ($cm^3\ g^{-1}$)	D_{Mean} (nm)	Degass. cond.	Pre-treat.	Impurities	Reference
Soth Tunisia	60	16	44	–	0.349	–	120^0	–	< (Q + Do)	Frini-Srasra and Srasra (2010)
Jebel Rheouis, Soth Tunisia	61	–	–	–	0.1444	74.34	–	< 100 μm	–	Allouche et al. (2020)
Huining, Gansu Province, China	61	9	52	0.0037	0.099	–	–	Powder	< (Q + M + Clh)	Zhang et al. (2015a)
Serradilla, Cáceres, Spain	71	–	–	–	0.14	–	–	Powder	~5% Q	Gonzalez et al. (1990)
Gafsa, Tunisia	75	–	–	–	0.136	72.34	–	< 2 μm*	< K	Ghrab et al. (2018)
Segovia	75	9	66	0.0042	0.1525	–	–	< 100 μm	–	Pardo-Canales et al. (2020)
Unknown	82	–	–	–	0.166	7.99	–	–	< Q	Huang et al. (2020)
Piaui State, Brazil	84	–	–	–	0.24	–	–	< 2 μm*	< Q	Oliveira et al. (2013)
Western Australia (unknown locality)	89	–	–	–	–	–	70^0-12 h	–	–	Sarkar et al. (2015)
Gaojiawa mine, Jiangsu Province, China	94	–	–	–	–	–	–	–	–	Wang et al. (2016)
Allow-Kagne, Senegal	100	14	86	0.0061	0.2047	–	–	< 100 μm	–	Pardo-Canales et al. (2020)
Maderuelo, Segovia, Spain	104	20	84	0.009	0.1896	–	–	< 100 μm	–	Pardo-Canales et al. (2020)
Piaui State, Brazil	106	–	–	–	–	–	200^0 12 h	< 74 μm	–	Araújo et al. (2020)
Senegal	106	21	85	0.0095	0.1933	–	–	< 100 μm	–	Pardo-Canales et al. (2020)
Torrejón, Cáceres, Spain	111	94	17	–	–	–	–	–	–	Hermosín and Cornejo (1986)
Piaui State, Brazil	112	–	–	–	–	–	–	< 20 μm	< K	Middea et al. (2018)
Jiangsu Province, China	122	–	–	–	0.34	–	–	< 74 μm	–	Shi et al. (2009)
Jiangsu Province, China	123	12.7	–	0.005	0.283	–	90^0 10 h	–	–	Zhang et al. (2010)
Ghoufi, Algeria	125	–	–	0.018	0.302	–	105^0 2 h	Soft acid	< Do	Boudriche et al. (2014, 2021)
Montgne de Reims, France	126	–	–	–	–	–	100^0	–	–	Cases et al. (1991)
China (unknown locality)	126	–	–	–	–	–	–	–	–	Lei et al. (2017)
Jiangsu Province, China	130	–	–	–	0.631	23.1	–	Powder	–	Yang et al. (2016)
South Africa (unknown locality)	131	–	–	–	–	–	–	–	–	Tichapondwa and Van Biljon (2019)
Sacramenia, Segovia, Spain	138	–	–	–	0.34	–	–	Powder	15% (Q + mica)	Gonzalez et al. (1990)
Jiangsu Province, China	138	–	–	–	–	6.07	–	–	–	Shi et al. (2020)
Anhui Province, China	139	–	–	–	0.22	–	–	Powder	< Q	Lai et al. (2010)
Anhui, China	141	31	110	0.014	0.43	–	–	–	–	Chen et al. (2019)
Unknown, China	141	87	–	0.04	0.17	2	–	–	–	Meng et al. (2021)
Pontezuela, Cuba	143	25	117	0.012	0.063	3.5	300^0 4 h	< 2 μm*	–	Alvarez et al. (2017)
China (unknown locality)	145	16	129	0.007	0.413	11.4	–	–	< Q	Guo et al. (2020)
Changzhou, China	145	–	–	–	0.301	41.57	300^0 2 h	–	< Q	Mou et al. (2021)
Jiangsu Province, China	147	–	–	–	–	–	–	–	< Q	Ouyang et al. (2018)
Ventzia basin, Macedonia, Greece	148	–	–	–	0.503	13.58	250^0 18 h	–	< (Q + Sm)	Bourliva et al. (2018)
Torrejón el Rubio, Cáceres, Spain	148	–	–	–	–	–	–	< 2 μm*	–	Vico and Acebal (2006)
Huai-An, China	149	–	–	–	0.218	3	–	Powder	–	Zhang et al. (2021)
Anhui Province, China	153	28	125	0.0012	0.39	–	–	Powder	< Q	Liu et al. (2012)
Western Australia (unknown locality)	153	–	–	–	0.218	6.9	–	Soft acid	–	Rusmin et al. (2016)
Ciudad Real, Spain	155	–	–	–	–	–	140^0 24 h	< 63 μm	–	Galán et al. (1994)
Piaui State, Brazil	156	–	–	0.01	0.36	13.8	–	< 20 μm*	–	Câmara et al. (2020)
Florida, U.S.A.	157	–	–	–	0.0815	–	–	< 45 μm*	< Q	Pushpaletha and Lalithambika (2011)
Soth Tunisia	158	–	–	–	–	–	–	< 2 μm*	~ 0	Hamdi et al. (2005)
Hyderabad, India	162	–	–	–	0.0826	–	–	< 45 μm*	< Q	Pushpaletha and Lalithambika (2011)
Gujarat, India	163	–	–	–	0.0841	–	–	< 45 μm*	< Do	Pushpaletha and Lalithambika (2011)
Jiangsu Province, China	164	–	–	–	–	–	–	–	~ 30% Q	Zeng et al. (2017)
Guanshan, Anhui Province, China	164	4	160	0	0.377	–	–	Powder	< Q	Zhang et al. (2015a)
Unknown	165	–	–	0.019	0.303	–	150^0 6 h	–	< Q	Yang et al. (2020)
Ciudad Real, Spain	170	–	–	–	–	–	140^0 24 h	< 63 μm	–	Galán et al. (1994)
Mingguang mine, Anhui province, China	171	44	127	–	–	–	–	–	–	Wang et al. (2019)
Attapulgus, Florida USA	173	–	–	–	–	–	–	–	–	Dogan et al. (2006)
Unkown	175	–	–	–	–	–	–	–	~ 25% (Q + Sm)	Gantenbein et al. (2011)

(*continued on next page*)

Table 1 (*continued*)

Geographical origin	SSA_{BET} ($m^2\ g^{-1}$)	$SA_{\mu p}$ ($m^2\ g^{-1}$)	SA_{ext} ($cm^2\ g^{-1}$)	$V_{\mu p}$ ($cm^3\ g^{-1}$)	Vt ($cm^3\ g^{-1}$)	D_{Mean} (nm)	Degass. cond.	Pre-treat.	Impurities	Reference
Jiangsu Province, China	175	31	144	0.013	0.4	–	–	–	–	Xu et al. (2014)
Karnataka, India	177	–	–	–	0.0898	–	–	< 45 µm*	< Q	Pushpaletha and Lalithambika (2011)
Huangnishan mine, Jiangsu Province, China	180	47	133	0.0214	0.265	5.86	–	Soft acid	< Q	Zhang et al. (2015b)
Jiangsu Province, China	181	–	–	–	–	9.74	–	–	~ 0	Zhong et al. (2019)
Xuyi, China	182	–	–	–	0.492	10.84	200^0 10 h	Powder	–	Yang et al. (2010)
Bercimuel, Segovia, Spain	186	–	–	–	–	–	–	Powder	~10% (Q + M)	Suárez-Barrios et al. (1995)
Lingshou, Hebei province, China	189	–	–	–	0.869	8.45	400^0 2 h	–	–	Miao et al. (2020)
Jiangsu Province, China	200	–	–	–	0.46	9.23	–	–	–	Xu et al. (2020)
Xuyu, Jiangsu Province, China	202	–	–	–	0.58	11.5	200^0	–	~ 0	Tian et al. (2020)
Huangnishan mine, Jiangsu Province, China	206	48	158	0.021	0.507	–	–	Powder	< Q	Zhang et al. (2015a)
China (unknown locality)	206	–	–	–	0.348	9.46	160^0 3 h	–	–	Liu et al. (2019)
Mingguang mine, Anhui Province, China	207	76	131	0.0347	0.3989	7.71	100^0 2 h	Powder	–	Wang et al. (2021)
Guanshan mine, Anhui province, China	213	–	–	–	–	–	90^0 12 h	< 75 µm	< (Q + Do)	Liu et al. (2014)
Attapulgus, Florida USA	221	112	124	–	–	–	140^0 2 h	Powder	< Sm	Sánchez del Río et al. (2009)
Ventzia Basin, Macedonia, Greece	225	57	168	0.0252	0.3232	–	–	< 100 µm	–	Pardo-Canales et al. (2020)
Ticul, Mexico	236	81	140	–	–	–	140^0 4 h	–	< Q	Sánchez del Río et al. (2009)
Anhui Province, China	239	96	143	–	0.36	5.96	–	–	~ 0	Lu et al. (2019)
Bercimuel, Segovia, Spain	254	–	–	–	–	–	–	–	–	Sanchez-Martin et al. (2006)
Xuji, Jiangsu Province, China	262	93	169	–	0.4	–	–	Soft acid	~ 0	Zhang et al. (2015c)
Ventzia basin, Macedonia, Greece	297	–	–	–	0.81	11	100^0 3 h	< 2 µm*	~ 0	Papoulis et al. (2013)

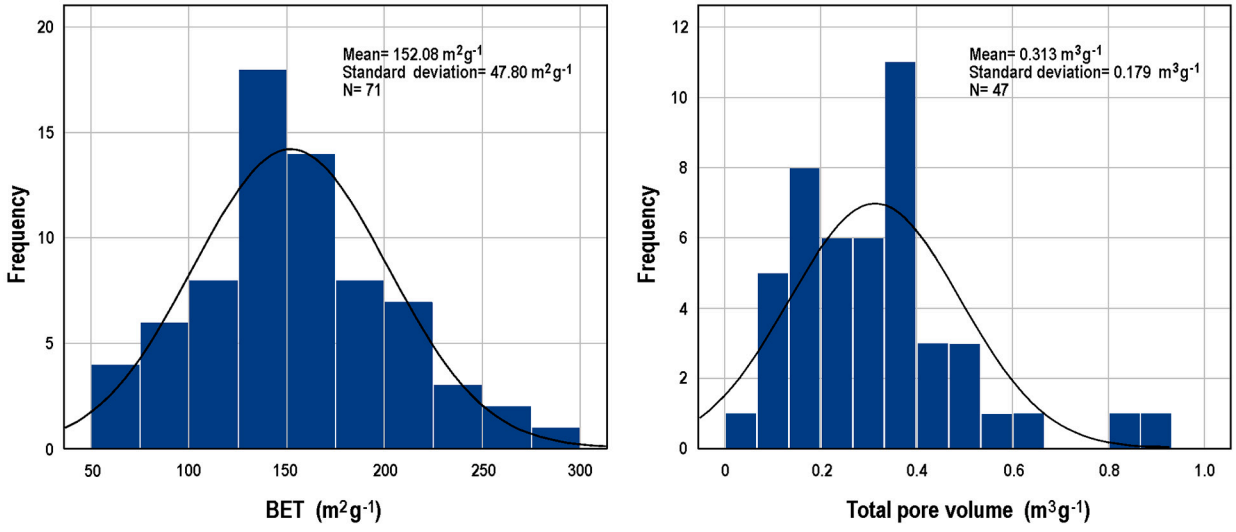

Fig. 1. a) Histogram of BET (in m^2g^{-1}) and b) histogram of total pore volume (in m^3g^{-1}), both from the data reported in the references collected in Table 1. b.

and external surface area data. In these samples, the microporosity ranges from only 4 m^2g^{-1} to 96 m^2g^{-1} for palygorskites from Guanshan and Anhui (China), as reported by Zhang et al. (2015a) and Lu et al. (2019), respectively, while the external surface area varies between 17 m^2g^{-1} and 169 m^2g^{-1} for palygorskites from Torrejón (Spain) and Jiangsu (China), as reported by Hermosín and Cornejo (1986) and Zhang et al. (2015c), respectively. This means that the microporosity can influence the final SSA in very different ways depending on the samples because it ranges from only 2.44% to 86.68% of the SSA. The mean value of microporosity recorded in Table 1 is 43.38 m^2g^{-1}, while the external surface area mean value is 112 m^2g^{-1}, and in most cases, the external surface area is higher than the micropore surface (Fig. 4). There are only two cases reported in Table 1 (Hermosín and Cornejo, 1986; Meng et al., 2021) that show higher values of micropore surface area than external surface, but in both cases, there is no information on the possible impurities nor on the pre-treatment and outgassing conditions used in order to evaluate how far the mineral structure and microstructure can be responsible of that different behaviour.

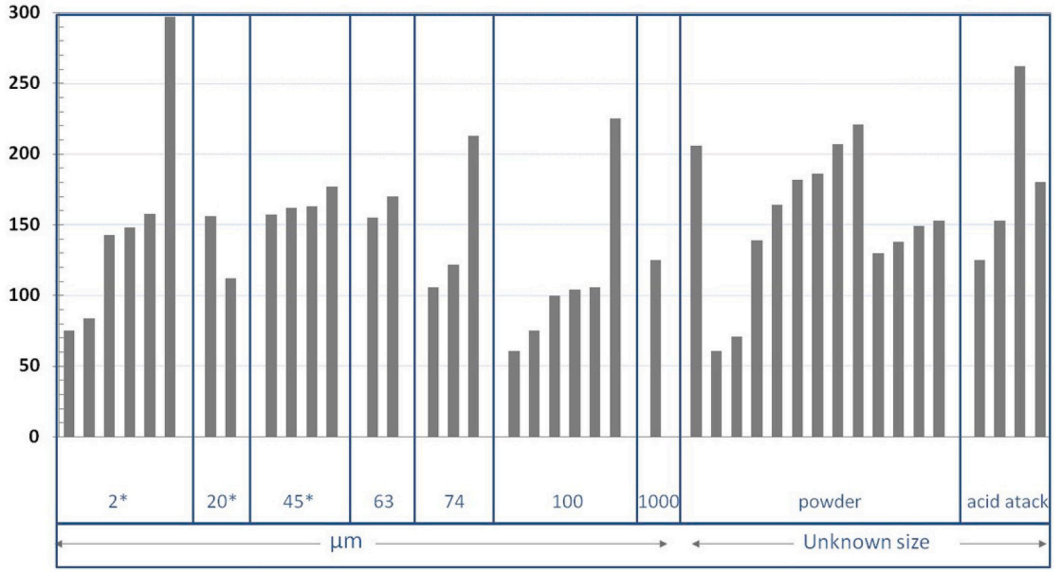

Fig. 2. BET data (in m^2g^{-1}) from the references collected in Table 1 plotted according to the size of the particles obtained after pre-treatment. Data with * correspond to fractions minor than the indicated value, as obtained from suspension in water, decantation and powdering.

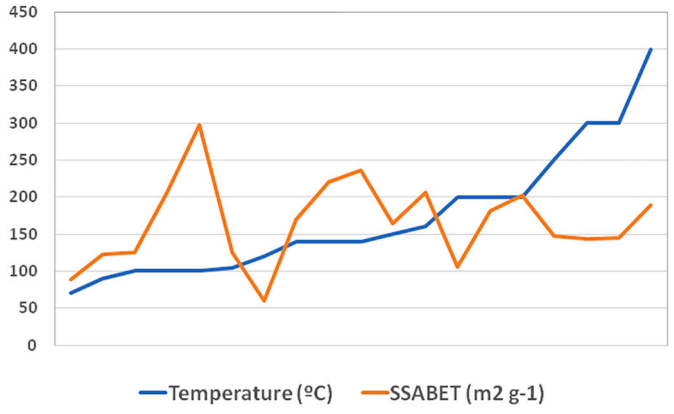

Fig. 3. SSA values and temperatures of outgassing from the date recorded in Table 2, plotted from the lowest to the highest temperature used for out-gassing.

Finally, very few references give data on the micropore volume or the mean pore diameter. However, the data of the total volume of pores are frequent, and a high variability is found again (Table 1 and Fig. 1b). Total volume of pores ranges from 0.063 cm^3g^{-1} to 0.869 cm^3g^{-1}, with a mean value of mean pore diameter is 16.84 nm, that is in the meso-porosity range according to the IUPAC. Clay minerals, in general, are characterized by a fractal distribution of their porosity, which ranges between the smaller micropores related to their crystal structure, as in smectites and sepiolite, to the macropores due to their microstructure (Přikryl and Weishauptová, 2010; Suárez and García-Romero, 2012).

2. Experimental

With the aim of studying the influence of the intrinsic properties of palygorskite, such as fibre size, crystallinity and microstructure, on the surface properties of palygorskite, a group of 22 high purity samples was chosen (Table 2). Some of these samples have been previously studied with other objectives in Suárez et al. (2007, 2018), García-Romero and Suárez (2010, 2013, 2014), Sánchez del Río et al. (2009), Suárez and García-Romero (2011, 2013) and Stathopoulou et al. (2011). On the other hand, some of the samples here studies have the same origin that some of those are in Table 1, which contains bibliographic references on the surface properties of palygorskite. The deposits that have been studied both in bibliography and in this work are form Attapulgus (U.S. A.), Bercimuel and Torrejón (Spain), and Ticul (Mexico).

The surface properties, including specific surface area (SSA), micropore surface area ($SSA_{\mu p}$), micropore volume ($V_{\mu p}$), external surface area (SSA_{Ex}) and mean equivalent pore diameter, were obtained from N_2 adsorption-desorption isotherms at −196 °C obtained from a static-volumetric apparatus (Micromeritics ASAP 2010 adsorption analyser). All samples were pre-treated and analysed in the same way, as follows: 0.3 g of the raw sample powdered in a manual mortar was outgassed for 4 h at 110 °C to reach a pressure of ≤3 µm Hg. The isotherms were obtained following a previously fixed 40-point P/P_0 table, and their reproducibility was checked. Samples were weighed prior to and after the vacuum thermal treatment of outgassing to determine the amount of water lost.

Thermal analyses were performed with simultaneous SDT-Q600 TA Instrument, equipment from ambient temperature to 1000 °C, with a rate of heating of 10 °C/min in air, with ~0.2 g of powdered sample in alumina crucible.

Scanning electron microscopy (SEM) observations were performed using a JEOL JSM 6400 microscope operating at 20 kV at the National Center of Electron Microscopy of Complutense University. Prior to the SEM-FEG examination, freshly fractured surfaces of representative samples were air-dried and coated with Au under vacuum.

3. Results and discussion

All N_2 isotherms obtained were similar in shape, as logical, because all samples were very rich in palygorskite (Fig. 5). According to this shape and the hysteresis loop, they could be classified as Type II of the IUPAC classification, which does not present limited adsorption at relative pressures close to the unit. On the other hand, most samples presented high adsorption at the lowest relative pressures, corresponding to microporous solids (Fig. 5). All the samples also presented very narrow hysteresis loops that are classified as Type A, which indicate the presence of tubular pores, according to De Boer and Lippens (1964).

Table 3 contains the data obtained from the N_2 isotherms of the studied palygorskites. As shown, there are significant differences among the samples, even in this group of very pure palygorskites in which the influence of minor amounts of impurities is negligible. The SSA_{BET} varies

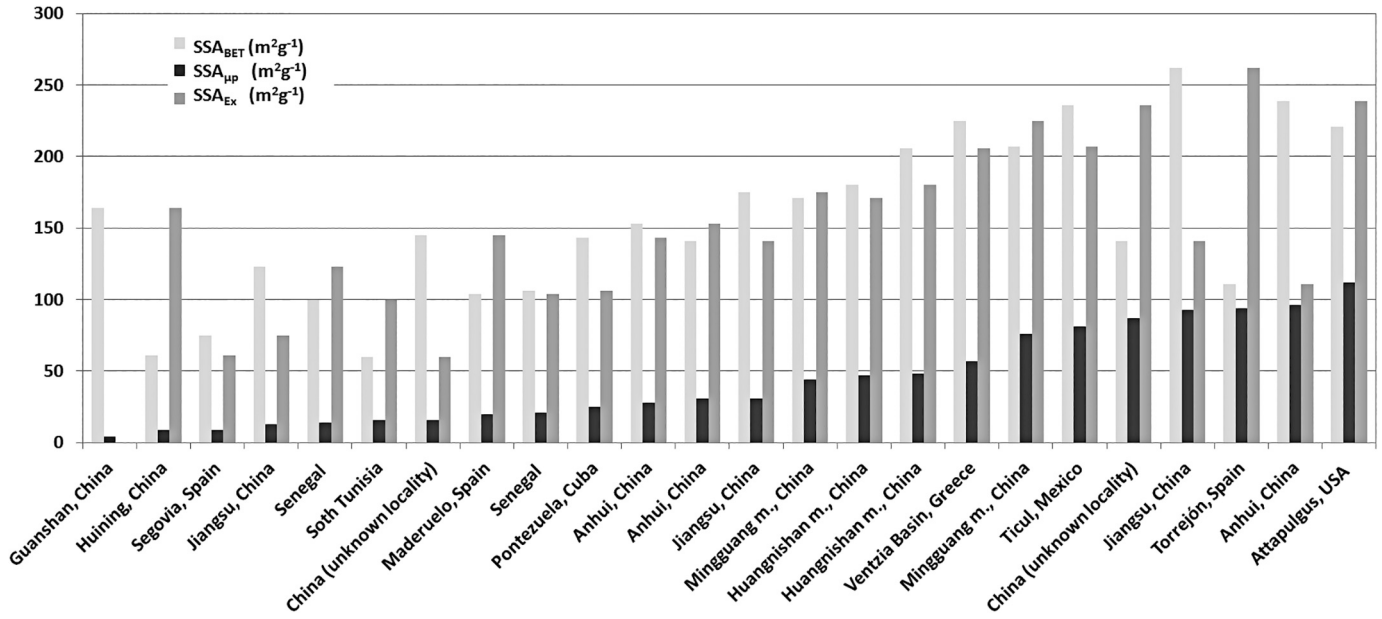

Fig. 4. Graphical representation of specific surface area (SSA$_{BET}$), micropore surface area (SSA$_{\mu p}$), and external surface area (SSA$_{Ex}$) data from Table 2, ordered from the lowest to the highest microporosity.

Table 2
Studied samples with their origin, label and impurities if there are.

Sample	Origin	Impurities	Sample	Origin	Impurities
ATT	Attapulgus (U.S.A)	smectite <5%	OKE	Okehampton (U.K.)	–
BER	Bercimuel (Spain)	illite + quartz <15%	PAL	Palygorskaya (Russia)	–
BOA	Boavista (Brasil)	–	PIC	Pics Crossing (Australia)	–
BUH	Buho (Spain)	–	SAL	Salamanca (Spain)	Illite + quartz <15%
CAS	Cassiar (Canada)	–	SEG	Segovia (Spain)	–
ESQ1	Esquivias (Spain)	quartz <5%	TEM	Tembleque (Spain)	Illite + quartz <10%
ESQ2	Esquivias (Spain)	quartz <5%	TOR	Torrejón (Spain)	quartz <5%
LEB	Lebrija (Spain)	quartz <5%	TRA	Trancos (Spain)	–
LIB	Lisbon (Portugal)	–	Y13	Yucatán (Mexico)	–
LIL	Lisboa (Portugal)	–	Y1A	Yucatán (Mexico)	–
NIJ	Nijar (Spain)	–	Y7	Yucatán (Mexico)	–

between 47 m^{2}g^{-1} and 269 m^{2}g^{-1}, in the same range as the values listed in Table 1, which indicates that such a large variation is characteristic of the mineral. These variations must be related to some intrinsic properties of the mineral in addition to the microstructure because in this study, they cannot be attributed neither to impurities nor to different pre-treatment and outgassing conditions. Additionally, the variations found among the values of SSA$_{Ext}$ and SSA$_{\mu m}$ are similar to those from the literature recorded in Table 1. The SSA$_{Ext}$ varies between 40 m^{2}g^{-1} and 190 m^{2}g^{-1}, whereas the SSA$_{\mu m}$ is between just 7 m^{2}g^{-1} and 123 m^{2}g^{-1}. In most samples analysed, as in the references, the SSA$_{\mu m}$ is lower than the SSA$_{Ext}$. Regarding the mean pore diameter (Table 3), there are no significant differences among the samples, and in all cases, the mean pore diameter is in the mesopore range, according to the IUPAC classification.

A classical question in studies of the surface properties of sepiolite-palygorskite fibrous clays is the accessibility of N_2 molecules to the inner part of intracrystalline tunnels. However, prior to this, it is necessary to know the availability of these tunnels after the outgassing process. To evaluate whether only zeolitic water or coordinated water was released under the vacuum and thermal conditions used, the weight of the samples was recorded before and after the outgassing process, and the loss of water, expressed as a percentage of the initial weight (LW%), was calculated. The LW% varies between 8.35% and 18.17%, with a mean value of 14.83%. These results were compared with the data obtained from the thermal analysis in a group of samples selected for this purpose. As shown in Fig. 6, the LW% during the outgassing process corresponds to equivalent temperatures much higher than 400 °C in TG analysis, the temperature at which the folding is complete according to different authors (Serna et al., 1977; VanScoyoc et al., 1979; Suárez and García-Romero, 2019). Although the ideal procedure would be to evacuate only zeolitic water, without releasing coordinated water and leaving the tunnels fully accessible, this is not possible under vacuum. To be able to achieve the relative pressures <1 Pa required for the microporous analyses, folding of the crystalline structure is inevitable; therefore, accessibility to the original intracrystalline tunnels is not possible, and their real internal microporosity cannot be known.

The accessibility of N_2 to the inner part of the tunnels is not only conditioned by the folding and the length of the fibre but also has a clear influence on the crystal chemistry and crystalline structure. Palygorskite is the term used for the minerals of the polysomatic series sepiolite-palygorskite closer to the extreme in which only palygorskite type polysomes appear and they diffract without sign of the presence of random sepiolite polysomes in their structure (Suárez and García-Romero, 2011, 2013), but in most cases palygorskitic minerals contain a variable proportion of sepiolite type polysomes, which implies: i) a higher proportion of Mg in their chemical composition because sepiolite polysomes only have Mg^{2+} as octahedral cations whereas palygorskite polysomes have the same number of octahedral positions occupied by Al^{3+} and Mg; ii) a proportion of wider tunnels into the crystals, with higher accessibility to the N_2, due to the wider size of the sepiolite polysomes. Based on these assumptions, the richer the Mg in the samples, the higher the SSA$_{BET}$. Table 4 contains the correlation coefficients (c.c.) between the textural parameters (SSA$_{BET}$, SSA$_{EXT}$, SSA$_{\mu p}$, V$_{\mu p}$, and

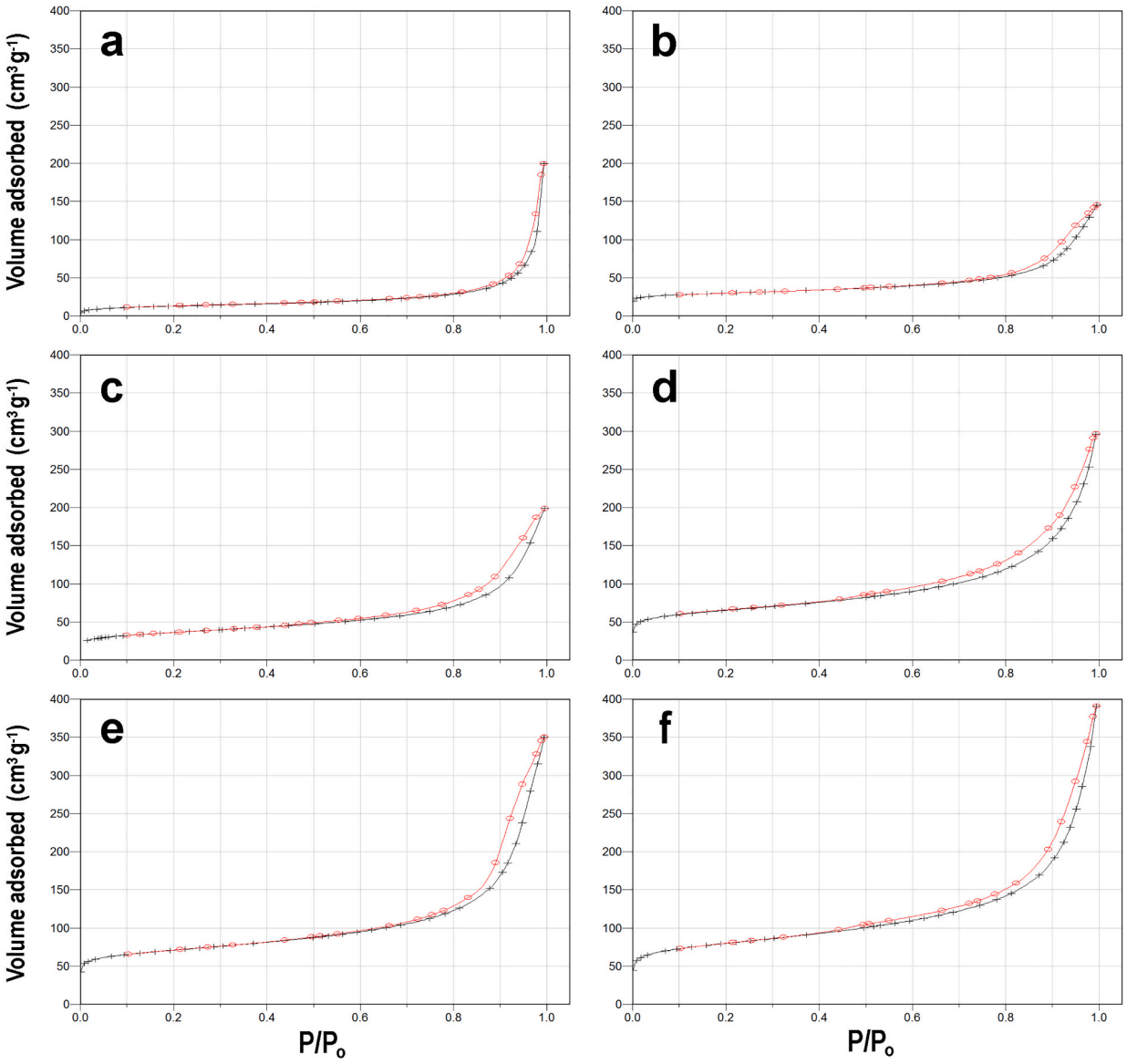

Fig. 5. N_2 adsorption-desorption isotherms of some representative samples.

DM) and the number of octahedral positions occupied by Mg (Table 3), according to the structural formulae of each sample published in García-Romero and Suárez (2010). There is a positive correlation between the SSA_{BET} and the content in Mg, with a c.c. = 0.641 and a high bilateral significance, but these data are even better when the microporosity is considered because the c.c. between the $SSA_{\mu p}$ and octahedral Mg is 0.682 with 0.001 of bilateral significance. This demonstrates that the palygorskite structure and its crystal chemistry also influence the surface properties, which is shown for the first time.

The absence of structural formula data in the references recorded in Table 1 makes it impossible to perform a similar statistical analysis. However, it is verifiable that the palygorskites from Table 1 with the highest values of SSA and microporosity are Mg-rich palygorskites. It is possible to deduce that through the X-ray diffraction (XRD) data reported in the references, the high content in Mg due to the presence of sepiolite polysomes in palygorskite produces high 011 and 200 d-spacing in the XRD patterns (Suárez et al., 2007; Stathopoulou et al., 2011; Suárez and García-Romero, 2011, 2013). The references of palygorskites with the highest SSA values recorded in Table 1 are those reported by Sanchez-Martin et al. (2006), Papoulis et al. (2013), Zhang et al. (2015c) and Lu et al. (2019), and in this paper, the 110 d-spacings of palygorskite reported from their XRD patterns are 10.54 Å, 10.53 Å, 10.6 Å, and 10.53 Å, respectively. These d-spacings indicate a high amount of octahedral Mg. At the opposite extreme, Gonzalez et al. (1990) described one of the samples with the lowest SSA in Table 1 (71 m^2g) as a very pure and aluminium-rich palygorskite, ratifying the influence of the crystal chemistry on the surface properties of palygorskite.

In addition to the accessibility to N_2 to the inner part of the tunnel, the size of the fibres and microstructure must also be considered. Both the size and microstructure can vary greatly (García-Romero and Suárez, 2013), and as an example, representative images of the microstructure of some palygorskites are shown in Fig. 7. These images can be used to explain the influence of the microstructure on the microporosity. The sample with the lowest SSA_{BET} and microporosity is CAS, which is a very pure palygorskite; therefore, the presence of impurities cannot be claimed to explain their low surface properties. The microstructure of the CAS sample can be observed in Fig. 7. First, the fibres are very long, so they have limited accessibility of N_2 molecules to the inner part of the tunnels. If N_2 is only able to penetrate at the "entrance" of the micropores, as longer the fibre is, lower the accessibility of N_2 for the same weight of palygorskite is. In other words, each time that one fibre is "divided" in two, the number of ends and consequently the accessibility

Table 3
Results from the adsorption study show that the samples are ordered from the lowest to the highest SSA_{BET}. LW%: lost weight percentage during the outgassing process. Data obtained from the N_2 analysis: specific surface area (SSA_{BET}), external surface area (SSA_{EXT}), micropore surface area ($SSA_{\mu p}$), micropore volume ($V_{\mu p}$), and mean pore diameter (DM). Mg^{VI}: number of octahedral positions occupied by Mg atoms in palygorskite (a.p.h.u.c. = atoms per half unit cell. nd: not determined.

Sample	LW %	SSABET	SSAEXT	SSAμp	Vμp	DM	MgVI
		m^2g^{-1}	m^2g^{-1}	m^2g^{-1}	cm^3g^{-1}	nm	a.p.h.u.c
CAS	14.47	47	40	7	0.004	19.52	1.79
NIJ	13.32	102	92	10	0.0056	19.9	2.1
SAL	13.91	104	45	59	0.0296	19.87	nd
TOR	8.35	105	51	54	0.0254	19.98	2.28
BUH	13.65	117	97	20	0.0094	nd	1.72
OKE	14.22	118	73	45	0.0235	20.1	1.88
LEB	11.81	135	117	18	0.0091	nd	1.66
LIB	15.46	157	73	83	0.0412	20.38	2.27
BER	12.99	168	92	76	0.018	20.09	1.98
PAL	14.45	173	120	53	0.0243	19.11	2.05
SEG	15.44	173	120	53	0.0481	20.21	1.85
BOA	12.93	175	96	79	0.0428	20.65	1.91
TEM	13.99	177	147	30	0.0147	20.03	1.97
Y7	16.54	181	123	58	0.0512	20.17	2.21
Y13	11.61	185	82	103	0.0536	20.18	2.34
PIC	13.69	208	85	123	0.0678	20.45	2.24
ATT	19.51	221	140	81	0.0512	20.06	2.31
Y1A	28.17	237	136	101	0.0523	20.17	2.54
TRA	16.71	251	143	94	0.0525	20.58	2.83
ESQ2	19.98	261	157	104	0.0584	20.14	2.92
ESQ1	13.72	264	150	114	0.056	19.8	3.34
LIL	17.81	289	190	99	0.0491	19.87	1.95

to the inner part of the tunnels double. The influence of the fibre length on the microporosity can be observed in Fig. 7, in which the samples are ordered from the longest to the shorter fibres, and they are also ordered from the lowest the highest microporosity.

On the other hand, the interfibre microporosity due to the close microstructure of the samples also plays an important role in the final values of SSA_{BET}, $SSA_{\mu p}$, and SSA_{EXT}. Cases et al. (1991) pointed out the existence of interfibre microporosity by studying the textural properties of palygorskite, and Suárez and García-Romero (2012) demonstrated that the microporosity of a group of sepiolites changed when the microstructure was modified. In the group of palygorskites studied here, the samples with minor microporosity not only have long fibres but also present very open textures, such as samples CAS and NIJ in Fig. 7, while samples such as Y13 and PIC, which have short rods in a closed microstructure, have the highest microporosity due both to the fibre length and to the interfibre microporosity.

4. Final remarks and conclusions

The review of a wide number of papers (71) focused on the surface properties of palygorskite reveals that this minerals has high variability of its surface properties. Extreme values of SSA are not related to extreme outgassing conditions or pre-treatment. The data from the bibliography and the results obtained from the study of 22 samples of very pure palygorskites show the very high variability of the surface properties of this relevant industrial mineral. This wide variation occurs for the specific surface area, micropore surface area, micropore volume, external surface area and mean equivalent pore diameter, and all these properties are influenced by several factors related both to the crystalline structure and to the microstructure.

The first conclusion is that even for soft outgassing conditions such as those used in this work, folding of the palygorskite crystalline structure is unavoidable, and accessibility to the inner part of the intracrystalline tunnels of N_2 molecules is limited.

On the other hand, while the SSA_{EXT} only depends on the microstructure, the microporosity is related to the crystalline structure, fibre length and microstructure because of the following reasons:

Table 4
Correlation coefficients (c.c.) between the textural parameters (SSA_{BET}, SSA_{EXT}, $SSA_{\mu p}$, $V_{\mu p}$, and DM) and the number of octahedral positions occupied by Mg per half unit cell.

	SSA_{BET}	SSA_{EXT}	$SSA_{\mu p}$	$V_{\mu p}$	DM	LW %
SSA_{EXT}	**.850****					
	0.000					
$SSA_{\mu p}$	**.807****	0.377				
	0.000	0.084				
$V_{\mu p}$	**.785****	.425*	**.906****			
	0.000	0.049	0.000			
DM	0.257	0.039	0.435	.510*		
	0.287	0.875	0.063	0.026		
LW %	.527*	.544*	0.342	0.418	0.081	
	0.017	0.013	0.140	0.067	0.750	
Mg^{VI}	**.641****	0.377	**.682****	**.635****	0.127	0.309
	0.002	0.092	0.001	0.002	0.617	0.199

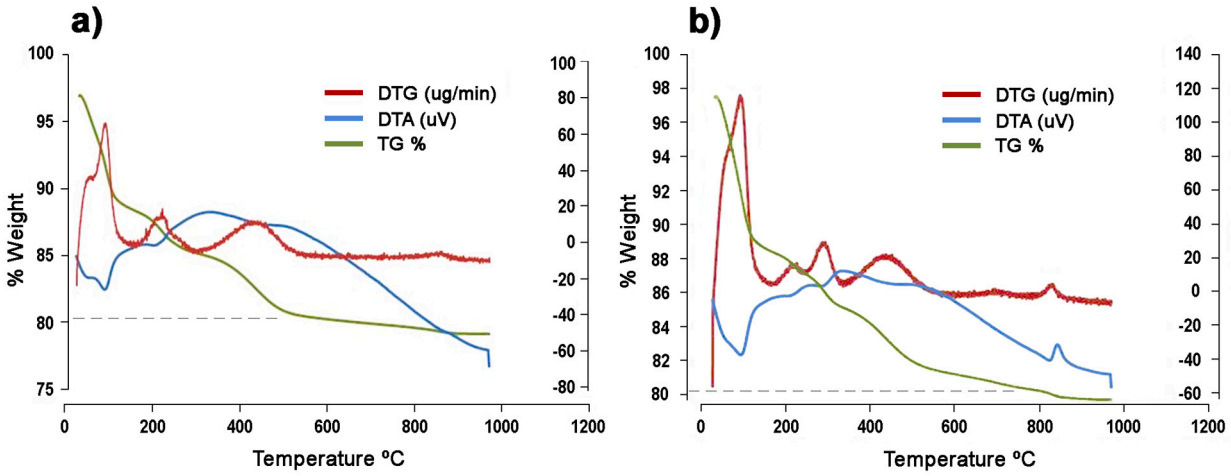

Fig. 6. Thermogravimetric analysis (green), derivate of the themogravimetric analysis (reed) and differential thermal analysis (blue) curves of a) ATT sample and b) E10 sample. Discontinuous lines indicate LW % (19.51% and 19.98%, respectively). (For interpretation of the references to colour in this figure legend, the reader is referred to the web version of this article.)

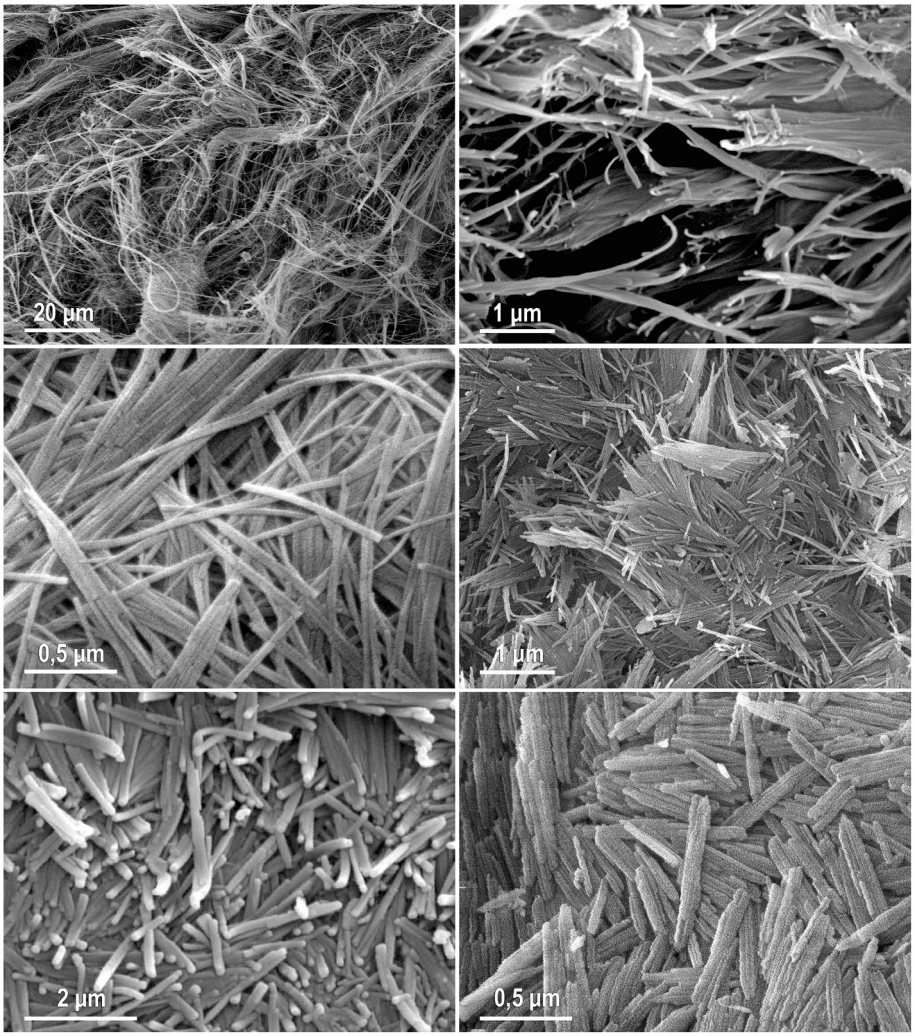

Fig. 7. Representative images of the microstructure and its relationship with the microporosity. The samples are ordered from the lowest to the highest microporosity: CAS = 7 m^2g^{-1}, NIJ =10 m^2g^{-1}, SEG = 53 m^2g^{-1}, ATT = 81 m^2g^{-1}, Y13 = 103 m^2g^{-1}, PIC = 123 m^2g^{-1}, and the fibres are progressively shorter and have a closer microstructure. Note the very different magnification of the images.

i) Magnesian palygorskites contain proportions of sepiolite polysomes in their crystalline structure, which implies a proportion of wider tunnels with more N_2 accessibility, and this is found here for the first time.
ii) The fibre length influences the partial accessibility of N_2 to intracrystalline tunnels because the shorter the fibre, the higher the number of edges and the partial accessibility to the entrance.
iii) The subparallel arrangement of the rods in fibre bundles generates inferfibre microporosity.

The first two are characteristic of each mineral depending on its geological origin, but the interfibre microporosity can be modified if the microstructure changes during the pre-treatment of the sample. All these factors can influence the sample in very different ways because the crystal chemistry and microstructural variations are very wide for this mineral, as shown in research by García-Romero and Suárez (2010, 2013). For this reason, there are wide variations of the surface properties like those described in this study, even for very pure palygorskitic samples. This implies that prior to the use of palygorskite in a certain industrial applications, it is necessary to study its surface properties considering the possible microstructure variations during industrial processes.

Authors statement

Conceptualization, writing draft, and funding acquisition: Mercedes Suárez and Emilia García-Romero. Analysis and discussion of results: all authors.

Declaration of Competing Interest

The authors declare that they have no known competing financial interests or personal relationships that could have appeared to influence the work reported in this paper.

Acknowledgments

Grant PID-2019-106504RB funded by MCIN/AEI/ 10.13039/501100011033.

References

Allouche, F., Eloussaief, M., Ghrab, S., Kallel, N., 2020. Clay material of an eocene deposit (Khanguet Rheouis, Tunisia): identification using geochemical and mineralogical characterization. Clay Clay Miner. 68, 262–272. https://doi.org/10.1007/s42860-020-00062-0.

Álvarez, A., Santarén, J., Esteban-Cubillo, A., Aparicio, P., 2011. Current industrial applications of palygorskite and sepiolite. Dev. Clay Sci. 3, 281–298.

Alvarez, E.D., Laffita, Y.M., Montoro, L.A., Della Santina Mohallem, N., Cabrera, H., Pérez, G.M., Frutis, M.A., Cappe, E.P., 2017. Electrical, thermal and electrochemical properties of disordered carbon prepared from palygorskite and cane molasses. J. Solid State Chem. 246, 404–411. https://doi.org/10.1016/j.jssc.2016.09.024.

Araújo, C.M., das Virgens Santana, M., do Nascimento Cavalcante, A., Nunes, L.C.C., Bertolino, L.C., de Sousa Brito, C.A.R., Barreto, H.M., Eiras, C., 2020. Cashew-gum-based silver nanoparticles and palygorskite as green nanocomposites for antibacterial applications. Mater. Sci. Eng. C 115, 110927. https://doi.org/10.1016/j.msec.2020.110927.

Boudriche, L., Chamayou, A., Calvet, R., Hamdi, B., Balard, H., 2014. Influence of different dry milling processes on the properties of an attapulgite clay, contribution of inverse gas chromatography. Powder Technol. 254, 352–363. https://doi.org/10.1016/j.powtec.2014.01.041.

Boudriche, L., Calvet, R., Chamayou, A., Hamdi, B., 2021. Influence of different wet milling on the properties of an attapulgite clay, contribution of inverse gas chromatography. Powder Technol. 378, 29–39. https://doi.org/10.1016/j.powtec.2020.09.045.

Bourliva, A., Sikalidis, A.K., Papadopoulou, L., Betsiou, M., Michailidis, K., Sikalidis, C., Filippidis, A., 2018. Removal of Cu $^{2+}$ and Ni $^{2+}$ ions from aqueous solutions by adsorption onto natural palygorskite and vermiculite. Clay Miner. 53, 1–15. https://doi.org/10.1180/clm.2017.1.

Brunauer, S., Emmett, P.H., Teller, E., 1938. Adsorption of gases in multimolecular layers. J. Am. Chem. Soc. 60, 309–319. https://doi.org/10.1021/ja01269a023.

Câmara, A.B.F., Sales, R.V., Bertolino, L.C., Furlanetto, R.P.P., Rodríguez-Castellón, E., de Carvalho, L.S., 2020. Novel application for palygorskite clay mineral: a kinetic and thermodynamic assessment of diesel fuel desulfurization. Adsorption 26, 267–282. https://doi.org/10.1007/s10450-019-00144-z.

Cases, J.M., Grillet, Y., François, M., Michot, L., Villierás, F., Yvon, J., 1991. Evolution of the porous structure and surface area of palygorskite under vacuum thermal treatment. Clay Clay Miner. 39, 191–201. https://doi.org/10.1346/CCMN.1991.0390211.

Chang, P.-H., Sarkar, B., Jiang, W.-T., Li, Z., 2019. Clay minerals for pharmaceutical waste water treatment. In: Mercurio, M., Sarkar, B., Langella, A. (Eds.), Modified Clay and Zeolite Nanocomposite Materials. Elsevier, pp. 167–196. https://doi.org/10.1016/B978-0-12-814617-0.00011-6.

Chen, H., Zhao, Y., Wang, A., 2007. Removal of Cu(II) from aqueous solution by adsorption onto acid-activated palygorskite. J. Hazard. Mater. 149, 346–354. https://doi.org/10.1016/j.jhazmat.2007.03.085.

Chen, Q., Zhu, R., Deng, L., Ma, L., He, Q., Du, J., Fu, H., Zhang, J., Wang, A., 2019. One-pot synthesis of novel hierarchically porous and hydrophobic Si/SiOx composite from natural palygorskite for benzene adsorption. Chem. Eng. J. 378, 122131. https://doi.org/10.1016/j.cej.2019.122131.

De Boer, J., Lippens, B.C., 1964. Studies on pore systems in catalysts II. The shapes of pores in aluminum oxide systems. J. Catal. 3, 38–43. https://doi.org/10.1016/0021-9517(64)90090-9.

Dogan, A.U., Dogan, M., Onal, M., Sarikaya, Y., Aburub, A., Wurster, D.E., 2006. Baseline studies of the Clay Minerals Society source clays: specific surface area by the Brunauer Emmett Teller (BET) method. Clay Clay Miner. 54, 62–66. https://doi.org/10.1346/CCMN.2006.0540108.

Frini-Srasra, N., Srasra, E., 2010. Acid treatment of south Tunisian palygorskite: Removal of Cd(II) from aqueous and phosphoric acid solutions. Desalination 250, 26–34. https://doi.org/10.1016/j.desal.2009.01.043.

Galán, E., Mesa, J.M., Sánchez, C., 1994. Properties and applications of palygorskite clays from Ciudad Real, Central Spain. Appl. Clay Sci. 9, 293–302. https://doi.org/10.1016/0169-1317(94)90006-X.

Gantenbein, D., Schoelkopf, J., Matthews, G.P., Gane, P.A.C., 2011. Determining the size distribution-defined aspect ratio of rod-like particles. Appl. Clay Sci. 53, 538–543. https://doi.org/10.1016/j.clay.2011.01.034.

García-Romero, E., Suárez, M., 2010. On the Chemical Composition of Sepiolite and Palygorskite. Clay Clay Miner. 58, 1–20. https://doi.org/10.1346/CCMN.2010.0580101.

García-Romero, E., Suárez, M., 2013. Sepiolite–palygorskite: Textural study and genetic considerations. Appl. Clay Sci. 86, 129–144. https://doi.org/10.1016/j.clay.2013.09.013.

García-Romero, E., Suárez, M., 2014. Sepiolite-palygorskite polysomatic series: Oriented aggregation as a crystal growth mechanism in natural environments. Am. Mineral. 99, 1653–1661. https://doi.org/10.2138/am.2014.4751.

Ghrab, S., Eloussaief, M., Lambert, S., Bouaziz, S., Benzina, M., 2018. Adsorption of terpenic compounds onto organo-palygorskite. Environ. Sci. Pollut. Res. 25, 18251–18262. https://doi.org/10.1007/s11356-017-9122-2.

Gonzalez, F., Pesquera, C., Blanco, C., Benito, I., Mendioroz, S., Pajares, J.A., 1990. Structural and textural evolution under thermal treatment of natural and acid-activated Al-rich and Mg-rich palygorskites. Appl. Clay Sci. 5, 23–36. https://doi.org/10.1016/0169-1317(90)90004-9.

Guo, H., Zhang, H., Li, Q., Peng, F., Xiong, L., Wang, C., Hu, A., Yao, S., Chen, X., 2020. Removal of Olefins from Reforming Aromatic Hydrocarbons over Metal-Halide-Modified Acid-Activated Palygorskite. Energy Fuel 34, 9463–9472. https://doi.org/10.1021/acs.energyfuels.0c01529.

Hamdi, N., Della, M., Srasra, E., 2005. Experimental study of the permeability of clays from the potential sites for acid effluent storage. Desalination 185, 523–534. https://doi.org/10.1016/j.desal.2005.04.055.

Hermosín, M.C., Cornejo, J., 1986. Methylation of Sepiolite and Palygorskite with Diazomethane. Clay Clay Miner. 34, 591–596. https://doi.org/10.1346/CCMN.1986.0340514.

Huang, C., Wang, Y., Gong, M., Wang, W., Mu, Y., Hu, Z.-H., 2020. α-MnO2/Palygorskite composite as an effective catalyst for heterogeneous activation of peroxymonosulfate (PMS) for the degradation of Rhodamine B. Sep. Purif. Technol. 230, 115877. https://doi.org/10.1016/j.seppur.2019.115877.

Juárez, E., Ronquillo de Jesús, E., Nieto-Camacho, A., Kaufhold, S., García-Romero, E., Suárez, M., Cervini-Silva, J., 2016. The role of sepiolite and palygorskite on the migration of leukocyte cells to an inflammation site. Appl. Clay Sci. 123, 315–319. https://doi.org/10.1016/j.clay.2016.01.034.

Kaufhold, S., Dohrmann, R., Klinkenberg, M., Siegesmund, S., Ufer, K., 2010. N2-BET specific surface area of bentonites. J. Colloid Interface Sci. 349, 275–282. https://doi.org/10.1016/j.jcis.2010.05.018.

Lai, S., Yue, L., Zhao, X., Gao, L., 2010. Preparation of silica powder with high whiteness from palygorskite. Appl. Clay Sci. 50, 432–437. https://doi.org/10.1016/j.clay.2010.08.019.

Lei, C., Zhu, X., Gao, W., Zhang, F., 2017. Adsorption characteristics of acidized attapulgite clay for methylene blue. Chin. J. Environ. Eng. 11, 885–891. https://doi.org/10.12030/j.cjee.201509236.

Liu, Y., Wang, W., Wang, A., 2012. Effect of dry grinding on the microstructure of palygorskite and adsorption efficiency for methylene blue. Powder Technol. 225, 124–129. https://doi.org/10.1016/j.powtec.2012.03.049.

Liu, H., Chen, T., Chang, D., Chen, D., Xie, J., Frost, R.L., 2014. Effect of palygorskite clay on pyrolysis of rape straw: an in situ catalysis study. J. Colloid Interface Sci. 417, 264–269. https://doi.org/10.1016/j.jcis.2013.11.041.

Liu, B., Li, Y., Duan, Y., Ding, T., Tang, Y., Zheng, C., 2019. Effect of supports on performance of Cu–Fe based catalysts for higher alcohols synthesis from syngas. React. Kinet. Mech. Catal. 128, 695–706. https://doi.org/10.1007/s11144-019-01667-w.

Liu, Y., Gao, X., Zhang, G., Xiao, Y., 2020. Functionalization of silk fabric using hyperbranched polymer coated attapulgite nanoparticles for prospective UV-resistance and antibacterial applications. Mater. Res. Express 7, 055008. https://doi.org/10.1088/2053-1591/ab8844.

López-Galindo, A., Viseras, C., Cerezo, P., 2007. Compositional, technical and safety specifications of clays to be used as pharmaceutical and cosmetic products. Appl. Clay Sci. 36, 51–63. https://doi.org/10.1016/j.clay.2006.06.016.

López-Galindo, A., Viseras, C., Aguzzi, C., Cerezo, P., 2011. Pharmaceutical and cosmetic uses of fibrous clays. In: Developments in Clay Science. Elsevier, pp. 299–324. https://doi.org/10.1016/B978-0-444-53607-5.00013-X.

López-Pacheco, C.P., Nieto-Camacho, A., Zarate-Reyes, L., García-Romero, E., Suárez, M., Kaufhold, S., Zepeda, E.G., Cervini-Silva, J., 2017. Sepiolite and palygorskite-underpinned regulation of mRNA expression of pro-inflammatory cytokines as determined by a murine inflammation model. Appl. Clay Sci. 137, 43–49. https://doi.org/10.1016/j.clay.2016.12.006.

Lu, Y., Wang, W., Wang, Q., Xu, J., Wang, A., 2019. Effect of oxalic acid-leaching levels on structure, color and physico-chemical features of palygorskite. Appl. Clay Sci. 183, 105301. https://doi.org/10.1016/j.clay.2019.105301.

Meng, F., Song, M., Chen, Y., Wei, Y., Song, B., Cao, Q., 2021. Promoting adsorption of organic pollutants via tailoring surface physicochemical properties of biomass-derived carbon-attapulgite. Environ. Sci. Pollut. Res. 28, 11106–11118. https://doi.org/10.1007/s11356-020-10974-y.

Miao, W., Gan, S., Li, X., Lv, Y., 2020. A triply synergistic method for palygorskite activation to effectively impregnate phase change materials (PCMs) for thermal energy storage. Appl. Clay Sci. 189, 105530. https://doi.org/10.1016/j.clay.2020.105530.

Middea, A., Spinelli, L., de Souza Junior, F.G., Neumann, R., Fernandes, T., Faulstich, F. R.L., Gomes, O., 2018. Magnetic polystyrene-palygorskite nanocomposite obtained by heterogeneous phase polymerization to apply in the treatment of oily waters. J. Appl. Polym. Sci. 135, 46162. https://doi.org/10.1002/app.46162.

Mou, H., Huang, X., Deng, Q., Lei, Q., Luo, H., Liang, J., Zhang, X., Zhang, T., Yao, X., Zhang, L., 2021. Preparation of graphene oxide-modified palygorskite nanocomposites for high-efficient removal of Co(II) from wastewater. Environ. Sci. Pollut. Res. 28, 1919–1932. https://doi.org/10.1007/s11356-020-07890-6.

Mu, B., Wang, A., 2016. Adsorption of dyes onto palygorskite and its composites: a review. J. Environ. Chem. Eng. 4, 1274–1294. https://doi.org/10.1016/j.jece.2016.01.036.

Oliveira, R.N., Acchar, W., Soares, G.D.A., Barreto, L.S., 2013. The increase of surface area of a Brazilian palygorskite clay activated with sulfuric acid solutions using a factorial design. Mater. Res. 16, 924–928. https://doi.org/10.1590/S1516-14392013005000075.

Oubagaranadin, J.U.K., Murthy, Z.V.P., 2011. Carbons and clays for heavy metals removal - a review of latest literature. In: Sherwin, J.A. (Ed.), Langmuir Monolayers in Thin Film Technology. Nova Science Publishers, Inc., UK, pp. 1–49.

Ouyang, J., Gu, W., Zhang, Y., Yang, H., Jin, Y., Chen, J., Jiang, J., 2018. CO2 capturing performances of millimeter scale beads made by tetraethylenepentamine loaded ultra-fine palygorskite powders from jet pulverization. Chem. Eng. J. 341, 432–440. https://doi.org/10.1016/j.cej.2018.02.040.

Papoulis, D., Komarneni, S., Panagiotaras, D., Nikolopoulou, A., Li, H., Yin, S., Tsugio, S., Katsuki, H., 2013. Palygorskite–TiO2 nanocomposites: part 1. Synthesis and characterization. Appl. Clay Sci. 83–84, 191–197. https://doi.org/10.1016/j.clay.2013.09.003.

Pardo-Canales, L., Essih, S., Cecilia, J.A., Domínguez-Maqueda, M., Olmo-Sánchez, M.I., Pozo-Rodríguez, M., Franco, F., 2020. Modification of the textural properties of palygorskite through microwave assisted acid treatment. Influence of the octahedral sheet composition. Appl. Clay Sci. 196, 105745. https://doi.org/10.1016/j.clay.2020.105745.

Přikryl, R., Weishauptová, Z., 2010. Hierarchical porosity of bentonite-based buffer and its modification due to increased temperature and hydration. Appl. Clay Sci. 47, 163–170. https://doi.org/10.1016/j.clay.2009.10.005.

Pushpaletha, P., Lalithambika, M., 2011. Modified attapulgite: an efficient solid acid catalyst for acetylation of alcohols using acetic acid. Appl. Clay Sci. 51, 424–430. https://doi.org/10.1016/j.clay.2010.12.033.

Ruiz-Hitzky, E., Aranda, P., Darder, M., Fernandes, F.M., 2013a. Fibrous clay mineral–polymer nanocomposites. In: Developments in Clay Science. Elsevier, pp. 721–741. https://doi.org/10.1016/B978-0-08-098258-8.00023-7.

Ruiz-Hitzky, E., Darder, M., Fernandes, F.M., Wicklein, B., Alcântara, A.C.S., Aranda, P., 2013b. Fibrous clays based bionanocomposites. Prog. Polym. Sci. 38, 1392–1414. https://doi.org/10.1016/j.progpolymsci.2013.05.004.

Rusmin, R., Sarkar, B., Biswas, B., Churchman, J., Liu, Y., Naidu, R., 2016. Structural, electrokinetic and surface properties of activated palygorskite for environmental application. Appl. Clay Sci. 134, 95–102. https://doi.org/10.1016/j.clay.2016.07.012.

Rutherford, D.W., Chiou, C.T., Eberl, D.D., 1997. Effects of exchanged cation on the microporosity of montmorillonite. Clay Clay Miner. 45, 534–543. https://doi.org/10.1346/CCMN.1997.0450405.

Sánchez del Río, M., Boccaleri, E., Milanesio, M., Croce, G., van Beek, W., Tsiantos, C., Chyssikos, G.D., Gionis, V., Kacandes, G.H., Suárez, M., García-Romero, E., 2009. A combined synchrotron powder diffraction and vibrational study of the thermal treatment of palygorskite–indigo to produce Maya blue. J. Mater. Sci. 44, 5524–5536. https://doi.org/10.1007/s10853-009-3772-5.

Sanchez-Martin, M.J., Rodriguez-Cruz, M.S., Andrades, M.S., Sanchez-Camazano, M., 2006. Efficiency of different clay minerals modified with a cationic surfactant in the adsorption of pesticides: Influence of clay type and pesticide hydrophobicity. Appl. Clay Sci. 31, 216–228. https://doi.org/10.1016/j.clay.2005.07.008.

Sarkar, B., Liu, E., McClure, S., Sundaramurthy, J., Srinivasan, M., Naidu, R., 2015. Biomass derived palygorskite–carbon nanocomposites: Synthesis, characterisation and affinity to dye compounds. Appl. Clay Sci. 114, 617–626. https://doi.org/10.1016/j.clay.2015.07.001.

Serna, C., VanScoyoc, G.E., Ahlrichs, J.L., 1977. Hydroxyl groups and water in palygorskite. Am. Mineral. 62, 784–792.

Shi, L., Yao, J., Jiang, J., Zhang, L., Xu, N., 2009. Preparation of mesopore-rich carbons using attapulgite as templates and furfuryl alcohol as carbon source through a vapor deposition polymerization method. Microporous Mesoporous Mater. 122, 294–300. https://doi.org/10.1016/j.micromeso.2009.03.016.

Shi, Y., Yan, Z., Xu, Y., Tian, T., Zhang, J., Pang, J., Peng, X., Zhang, Q., Shao, M., Tan, W., Li, H., Xiong, Q., 2020. Visible-light-driven AgBr–TiO2-Palygorskite photocatalyst with excellent photocatalytic activity for tetracycline hydrochloride. J. Clean. Prod. 277, 124021. https://doi.org/10.1016/j.jclepro.2020.124021.

Stathopoulou, E.T., Suárez, M., García-Romero, E., Sánchez del Río, M., Kacandes, G.H., Gionis, V., Chryssikos, G.D., 2011. Trioctahedral entities in palygorskite: Near-infrared evidence for sepiolite-palygorskite polysomatism. Eur. J. Mineral. 23, 567–576. https://doi.org/10.1127/0935-1221/2011/0023-2112.

Suárez, M., García-Romero, E., 2011. Advances in the crystal chemistry of sepiolite and palygorskite. In: Developments in Clay Science. Elsevier, pp. 33–65. https://doi.org/10.1016/B978-0-444-53607-5.00002-5.

Suárez, M., García-Romero, E., 2012. Variability of the surface properties of sepiolite. Appl. Clay Sci. 67–68, 72–82. https://doi.org/10.1016/j.clay.2012.06.003.

Suárez, M., García-Romero, E., 2013. Sepiolite–Palygorskite: a Continuous Polysomatic Series. Clay Clay Miner. 61, 461–472. https://doi.org/10.1346/CCMN.2013.0610505.

Suárez, M., García-Romero, E., 2019. Comments on "Influence of thermally modified palygorskite on the viability of polycyclic aromatic hydrocarbon-degrading bacteria" by B. Biswas, B. Sarkar, and R. Naidy Applied Clay Science 134 (2016) 153–160. Appl. Clay Sci. 175, 197–198. https://doi.org/10.1016/j.clay.2017.04.012.

Suárez, M., García-Romero, E., Sánchez del Río, M., Martinetto, P., Dooryhée, E., 2007. The effect of the octahedral cations on the dimensions of the palygorskite cell. Clay Miner. 42, 287. https://doi.org/10.1180/claymin.2007.042.3.02.

Suárez, M., García-Rivas, J., García-Romero, E., Jara, N., 2016. Mineralogical characterisation and surface properties of sepiolite from Polatli (Turkey). Appl. Clay Sci. 131, 124–130. https://doi.org/10.1016/j.clay.2015.12.032.

Suárez, M., García-Rivas, J., Sánchez-Migallón, J.M., García-Romero, E., 2018. Spanish palygorskites: geological setting, mineralogical, textural and crystal-chemical characterization. Eur. J. Mineral. 30, 733–746. https://doi.org/10.1127/ejm/2018/0030-2753.

Suárez-Barrios, M., Flores-González, L.V., Vicente-RodríguezRodríguez, M.A., Martín-Pozas, J.M., 1995. Acid activation of a palygorskite with HCl: Development of physico-chemical, textural and surface properties. Appl. Clay Sci. 10, 247–258. https://doi.org/10.1016/0169-1317(95)00007-Q.

Tavanaee, M., Shirvani, M., Bakhtiary, S., 2017. Adhesion of *Pseudomonas putida* onto palygorskite and sepiolite clay minerals. Geomicrobiol J. 34, 677–686. https://doi.org/10.1080/01490451.2016.1238982.

Thommes, M., Kaneko, K., Neimark, A.V., Olivier, J.P., Rodriguez-Reinoso, F., Rouquerol, J., Sing, K.S.W., 2015. Physisorption of gases, with special reference to the evaluation of surface area and pore size distribution (IUPAC Technical Report). Pure Appl. Chem. 87, 1051–1069. https://doi.org/10.1515/pac-2014-1117.

Tian, H., Yao, J., Zha, F., Yao, L., Chang, Y., 2020. Catalytic activity of SAPO-34 molecular sieves prepared by using palygorskite in the synthesis of light olefins via CO2 hydrogenation. Appl. Clay Sci. 184, 105392. https://doi.org/10.1016/j.clay.2019.105392.

Tichapondwa, S.M., Van Biljon, J.B., 2019. Adsorption of Cr (VI) Pollutants in Water using Natural and Modified Attapulgite Clay. Chem. Eng. Trans. 74, 355–360. https://doi.org/10.3303/CET1974060.

VanScoyoc, G.E., Serna, C.J., Ahlrichs, J.L., 1979. Structural changes in palygorskite during dehydration and dehydroxylation. Am. Mineral. 64, 215–223.

Vicente-Rodríguez, M.A., Suarez, M., Bañares-Muñoz, M.A., de Dios Lopez-Gonzalez, J., 1996. Comparative FT-IR study of the removal of octahedral cations and structural modifications during acid treatment of several silicates. Spectrochim. Acta A Mol. Biomol. Spectrosc. 52, 1685–1694. https://doi.org/10.1016/S0584-8539(96)01771-0.

Vico, L., Acebal, S., 2006. Some aspects about the adsorption of quinoline on fibrous silicates and Patagonian saponite. Appl. Clay Sci. 33, 142–148. https://doi.org/10.1016/j.clay.2006.03.012.

Wang, W., Wang, A., 2016. Recent progress in dispersion of palygorskite crystal bundles for nanocomposites. Appl. Clay Sci. 119, 18–30. https://doi.org/10.1016/j.clay.2015.06.030.

Wang, W., Tian, G., Zhang, Z., Wang, A., 2016. From naturally low-grade palygorskite to hybrid silicate adsorbent for efficient capture of Cu(II) ions. Appl. Clay Sci. 132–133, 438–448. https://doi.org/10.1016/j.clay.2016.07.013.

Wang, W., Dong, W., Tian, G., Sun, L., Wang, Q., Hui, A., Mu, B., Wang, A., 2019. Highly efficient self-template synthesis of porous silica nanorods from natural palygorskite. Powder Technol. 354, 1–10. https://doi.org/10.1016/j.powtec.2019.05.075.

Wang, S., Ren, H., Lian, W., Wang, J., Zhao, Y., Liu, Y., Zhang, T., Kong, L.B., 2021. Purification and dissociation of raw palygorskite through wet ball milling as a carrier to enhance the microwave absorption performance of Fe3O4. Appl. Clay Sci. 200, 105915. https://doi.org/10.1016/j.clay.2020.105915.

Xu, J., Wang, W., Wang, A., 2014. Enhanced microscopic structure and properties of palygorskite by associated extrusion and high-pressure homogenization process. Appl. Clay Sci. 95, 365–370. https://doi.org/10.1016/j.clay.2014.02.011.

Xu, N., Zhou, R., Jiang, Q., Kong, L., Lei, H., 2020. GEO-PGS composite shows synergistic and complementary effect on Escherichia coli and improvement of intestinal dysfunction. Food Chem. Toxicol. 135, 110936. https://doi.org/10.1016/j.fct.2019.110936.

Yang, H., Tang, A., Ouyang, J., Li, M., Mann, S., 2010. From Natural Attapulgite to Mesoporous Materials: Methodology, Characterization and Structural Evolution. J. Phys. Chem. B 114, 2390–2398. https://doi.org/10.1021/jp911516b.

Yang, D., Peng, F., Zhang, H., Guo, H., Xiong, L., Wang, C., Shi, S., Chen, X., 2016. Preparation of palygorskite paraffin nanocomposite suitable for thermal energy storage. Appl. Clay Sci. 126, 190–196. https://doi.org/10.1016/j.clay.2016.03.014.

Yang, S., Xu, D., He, S., Yan, W., Xiong, Y., 2020. Modified Fe-rich palygorskite as an efficient and low-cost heterogeneous fenton catalyst for NO $_x$ and SO $_2$ removal. Energy Fuel 34, 8493–8502. https://doi.org/10.1021/acs.energyfuels.9b04459.

Zeng, H.F., Lin, L.J., Xi, Y.M., Han, Z.Y., 2017. Effects of raw and heated palygorskite on rumen fermentation in vitro. Appl. Clay Sci. 138, 125–130. https://doi.org/10.1016/j.clay.2017.01.006.

Zhang, J., Wang, Q., Chen, H., Wang, A., 2010. XRF and nitrogen adsorption studies of acid-activated palygorskite. Clay Miner. 45, 145–156. https://doi.org/10.1180/claymin.2010.045.2.145.

Zhang, Z., Wang, W., Wang, A., 2015a. High-pressure homogenization associated hydrothermal process of palygorskite for enhanced adsorption of Methylene blue. Appl. Surf. Sci. 329, 306–314. https://doi.org/10.1016/j.apsusc.2014.12.187.

Zhang, Y., Wang, W., Zhang, J., Liu, P., Wang, A., 2015b. A comparative study about adsorption of natural palygorskite for methylene blue. Chem. Eng. J. 262, 390–398. https://doi.org/10.1016/j.cej.2014.10.009.

Zhang, Y., Fan, L., Chen, H., Zhang, J., Zhang, Y., Wang, A., 2015c. Learning from ancient Maya: Preparation of stable palygorskite/methylene blue@SiO2 Maya Blue-like pigment. Microporous Mesoporous Mater. 211, 124–133. https://doi.org/10.1016/j.micromeso.2015.03.002.

Zhang, T., Wang, W., Zhao, Y., Bai, H., Wen, T., Kang, S., Song, G., Song, S., Komarneni, S., 2020. Removal of heavy metals and dyes by clay-based adsorbents: from natural clays to 1D and 2D nano-composites. Chem. Eng. J. 420 (Part 2), 127574. https://doi.org/10.1016/j.cej.2020.127574.

Zhang, N., Guo, H., Xiong, L., Zhang, H., Chen, X., 2021. Preparation and characterization of paraffin/palygorskite shape-stable composite phase change materials for thermal energy storage. J. Energy Storage 34, 102189. https://doi.org/10.1016/j.est.2020.102189.

Zhong, L., Tang, A., Yan, P., Wang, J., Wang, Q., Wen, X., Cui, Y., 2019. Palygorskite-template amorphous carbon nanotubes as a superior adsorbent for removal of dyes from aqueous solutions. J. Colloid Interface Sci. 537, 450–457. https://doi.org/10.1016/j.jcis.2018.11.016.

Zhong, H., Mu, B., Zhang, M., Hui, A., Kang, Y., Wang, A., 2020. Preparation of effective carvacrol/attapulgite hybrid antibacterial materials by mechanical milling. J. Porous. Mater. 27, 843–853. https://doi.org/10.1007/s10934-020-00863-7.